Kinetic study of coupled field-induced aggregation and sedimentation processes arising in magnetic fluids

F. Martínez-Pedrero,[1] A. El-Harrak,[2] J. C. Fernández-Toledano,[1] M. Tirado-Miranda,[1] J. Baudry,[2] A. Schmitt,[1] J. Bibette,[2] and J. Callejas-Fernández[1,*]

[1]*Department of Applied Physics, University of Granada, Campus de Fuentenueva, E-18071 Granada, Spain*

[2]*Laboratoire Colloïdes et Matériaux Divisés, ParisTech, ESPCI, UMR 7612, 10 rue Vauquelin, Paris F-75005 France*

(Received 5 December 2007; revised manuscript received 21 March 2008; published 17 July 2008)

In this work, the kinetics of coupled aggregation and sedimentation processes arising in magnetic fluids has been studied. Aggregation was induced applying a constant uniaxial magnetic field. The time evolution of the cluster-size distribution and the weight-average chain length was monitored using optical microscopy and digital image analysis. The experimental results are compared with the corresponding solutions of Smoluchowski's equation. For this purpose, a recently proposed aggregation kernel was employed. When sedimentation effects are taken into account, the fits improve especially at long aggregation times.

DOI: 10.1103/PhysRevE.78.011403 PACS number(s): 82.70.Dd, 61.43.Hv, 47.65.Cb

I. INTRODUCTION

Electro- and magnetorheological (MR) fluids are colloidal dispersions of small (micron-sized) particles that present a dipolar interaction when an external field is applied. When the field is present, the particles experience an attractive force along the field direction and a repulsive force normal to it. The strength of these interactions is tunable through the strength of the external field. When the particles are allowed to aggregate, linear aggregates are formed due to the anisotropic character of the dipolar interaction. The axes of the pearl-chain-like clusters are aligned along the field direction. At relatively high particle concentrations, even more complex structures may arise [1].

Due to their response to external fields, dispersions of dipolar particles and linear aggregates thereof have special physicochemical properties that make them very suitable for a growing number of applications in different fields such as biomedical applications, rheology, microfluids, light transmission devices, etc… (Ref. [2], and references therein). Moreover, chainlike aggregates that are able to survive in the absence of the applied field have given rise to new applications such as "artificial swimmers," microfluidic mixers, or instruments for proving the kinetics of adhesive processes [3–5]. Therefore, MR fluids are nowadays considered as an exciting class of smart materials.

The microstructure of MR fluids plays a significant role for their bulk rheological properties, and evidently, an adequate modeling of chain formation processes is of practical importance for the control of technological applications. So far, however, only a relatively small number of experimental and simulation studies address this topic, i.e., the formation of linear aggregates through field-induced aggregation processes in dipolar colloidal dispersions [6–10]. Moreover, most of these works focus on structural and scaling aspects. A detailed study of the aggregation kinetics and the time evolution of the cluster-size distribution is usually not performed. The kinetic information given is commonly limited to the asymptotic behavior of the average cluster size that shows a power-law dependency at long aggregation times.

However, the influence of phenomena and parameters such as sedimentation effects, electrostatic interparticle interactions, the strength of the applied field, or the degree of magnetic saturation of the particles are still not completely understood. Promislow *et al.*, propose that the kinetic parameter of the aggregation processes decreases with increasing field strength. Furthermore, they have shown that the aggregation time scale explicitly depends on the strength of the applied field [7]. More recently our team studied the influence of isotropic electrostatic interactions on the aggregation behavior of electric double layered magnetic particles by changing the electrolyte concentrations in the aqueous dispersion medium [10,11]. In our case, the average cluster size also followed a power law with an electrolyte independent kinetic exponent. This allowed us to conclude that the aggregation mechanism was completely controlled by the dipolar interaction. The absolute values of the cluster growth rates, however, were found to depend on the amount of electrolyte added, i.e., on the range of the total interaction between the particles. Hence, we proposed an aggregation kernel that explicitly includes the range of the effective interparticle interaction as a control parameter and so, depends implicitly on the interplay between the electrostatic and the magnetic interactions.

On a different vein, for typical practical applications, suspensions of composite magnetic nanoparticles are frequently employed. These particles often contain small grains of iron oxides which increase their relative density with regard to the dispersion medium. Both effects, the relatively high particle mass density and the increased size due to chain formation, favor differential sedimentation, i.e., small magnetic particles remain suspended while the large aggregates sink. Therefore, the study of MR fluids in the Earth's gravitational field is not straightforward. In order to overcome this difficulty, some studies have even been performed at the International Space Station [12]. Sedimentation is a serious problem for many manufacturers of technological applications, and gravitational effects must not be omitted for a correct description and modeling of this type of aggregation process.

*jcalleja@ugr.es

A further effect that should not be neglected *a priori* is mutual induction of the chain forming particles. At weak field strengths, the degree of magnetization of the particles is proportional to the local field strength and so, the net magnetization of the particles contained within a chain is enhanced by the presence of neighboring particles [13]. This effect leads to an increased range of the magnetic interaction between the aggregates as they gain in size.

The aim of this work is to deepen our knowledge about chain formation processes and to improve the theoretical description of field-induced aggregation phenomena when sedimentation plays a significant role. Therefore, we determine the time evolution of the cluster-size distribution and the average cluster size arising in aggregating magnetic particle dispersions and use the experimental data to test theoretical models based on Smoluchowski's approach. For this purpose, it will be essential to determine an aggregation kernel that includes all the effects mentioned above. Solving the corresponding Smoluchowski equation allows the experimental cluster-size distributions to be compared with the theoretical predictions. An improved understanding of the complex properties of MR fluids and the interactions of the particles contained therein, will undoubtedly help scientists to develop more sophisticated tools and methods for adequate control of a variety of industrial processes and devices that are based on such fluids.

II. THEORY

In dilute aggregating systems, it may be safely assumed that only binary collisions take place. Then, the time evolution of the cluster-size distribution can be described in the framework of the Smoluchowski equation that is given by

$$\frac{dX_n}{dT} = \frac{1}{2}\sum_{i+j=n} K_{ij}X_i(T)X_j(T) - X_n(T)\sum_{i=1}^{\infty} K_{\mathrm{in}}X_i(T), \qquad (1)$$

where X_n is the concentration of clusters c_n containing n primary particles normalized by the initial monomer concentration c_0. The normalized aggregation time $T=t/t_{\mathrm{agg}}$ is scaled by the characteristic aggregation time $t_{\mathrm{agg}}=2/(c_0k_s)$ for pure diffusion controlled aggregation where $k_s=12.3\times10^{-18}$ $\mathrm{m^3\,s^{-1}}$ is Smoluchowski's kinetic rate constant for aqueous media at 298 K [14]. Smoluchowski's theory is a mean field approach that describes the time evolution of the cluster-size distribution in terms of kinetic rate equations. The aggregation kernel $K_{ij}=2k_{ij}/k_{11}$ is normalized by the dimer formation rate constant k_{11}. It gives an orientational and configurational average for the exact aggregation rate constants k_{ij} for the reaction between i- and j-size clusters. All the physical information regarding the diffusive transport mechanism and the physicochemical interparticle interactions are contained in the kernel [15].

Pure diffusion-limited aggregation of noninteracting sticky particles may be described in terms of the so-called Brownian kernel that is given by

$$k_{ij}^{\mathrm{Br}} = 4\pi(a_i + a_j)(D_{ij}), \qquad (2)$$

where $D_{ij}=D_i+D_j$ is the mutual particle diffusion coefficient. It was derived considering solid spheres of radius a_i and a_j that undergo Brownian motion and stick as soon as they come into contact, i.e., when their center to center distance becomes a_i+a_j.

At low concentrations, chainlike aggregates of dipolar magnetic particles also undergo free diffusive motion until they reach the area of influence of another aggregate. When the interaction is attractive, the particle motion becomes ballistic and the linear aggregate snaps into position at the end of the other chain. Otherwise, the chains repel each other and diffuse away or eventually reach the attractive zone. Based on the Brownian kernel, Miyazima *et al.* proposed the power-law-type kernel $k_{ij}\propto(i^{\gamma}+j^{\gamma})$ for describing the aggregation of dipolar particles that are aligned under the influence of an external field [6]. This kernel contains two fundamental assumptions: (i) the collision cross section of the linear aggregates is independent of the cluster size and (ii) the diffusion coefficient of linear aggregates may be approximated by a power law of the cluster size, i.e., by $D_i\approx i^{\gamma}$.

In a recent work, we derived a kernel for magnetic-field-induced aggregation that considers explicitly not only the long-range character but also the anisotropic nature of the magnetic dipole-dipole interactions among the particles. This kernel is given by

$$k_{ij}^{\mathrm{mag}} = 4\pi(1-\cos\varphi_c)(2a+\bar{h})(\bar{D}_i+\bar{D}_j). \qquad (3)$$

In order to include the long-range character of the net interaction among two approaching particles of radius a, we define an effective interaction range $\bar{h}$ that is averaged over an entire attractive region. For interacting magnetic dipoles, this zone has a dumbbell-like shape and fits in a symmetric double cone with an aperture angle of $\varphi_c\approx55°$ with respect to the field direction. The diffusion coefficient of the linear aggregates has been approximated by the average translational diffusion $\bar{D}$ of rigid rods of length $L=2aN$, which is given by [16]

$$\bar{D}_N = \frac{k_BT}{6\pi\eta aN}[\ln(N)+0.312+0.565/N+(0.100/N)^2]. \qquad (4)$$

Here the chain length is expressed in terms of the number of monomeric particles N contained in the chain, k_BT is the thermal energy, and η is the viscosity of the liquid phase.

The aggregation kernel given by Eq. (3) has to be understood as a mean field approach using effective quantities such as the effective interaction range $\bar{h}$ and the effective diffusion coefficients $\bar{D}_i$ and $\bar{D}_j$. It should be noted that the only freely adjustable parameter is the effective interaction range $\bar{h}$. Further details about this kernel can be found in Ref. [10].

III. MATERIALS AND METHODS

The samples used for the experiments were aqueous suspensions of superparamagnetic core shell silica microspheres. The particles were produced starting from an

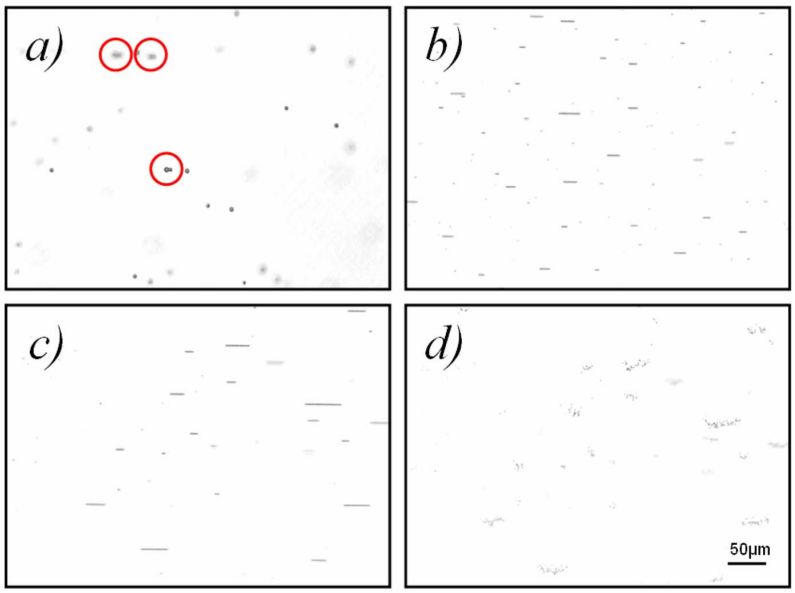

FIG. 1. (Color online) Optical micrographs of the magnetorheological suspension: (a) High magnification (20×) image taken at 1 s after application of the magnetic field. The circled dimers have formed mainly due to immediate ballistic aggregation of two initially close monomers. [(b) and (c)] Low magnification (10×) images taken at 250 and 495 s after taking on the magnetic field, respectively. Linear aggregates of different length aligned along the field direction are clearly visible. (d) Low magnification image (10×) of the situation shown in image (c) at 5 s after turning the field off. The chains disassemble into individual monomers.

octane-based ferrofluid containing 80% by weight of oleic acid covered Fe_2O_3 nanoparticles. To this, tetraethylortosilicate (TEOS) was added (8% by weight). In the next step, 80 g of a ferrofluid/TEOS mixture was added dropwise to 15 g of an aqueous solution of sodium alginate (2% by weight) and SDS (2% by weight). The premix was scantily sheared during its preparation. The resulting brownish paste was transferred to a Couette cell where it was sheared at 600 rpm in a 100 μm gap with a maximum injection rate of 7 mm/min. The solution obtained was then placed in a rotavapor at 50 °C under vacuum conditions in order to eliminate the octane content from the emulsion droplets. Afterwards, 50 ml of a 50/50 mixture of ammoniac and isopropanol were added dropwise in order to hydrolyze the TEOS. After 3 h of mechanical stirring, the particles were separated from the suspension medium by means of a magnet and washed several times with pure water. Finally, the particle surface was reinforced by increasing the thickness of the silica shell. This was achieved using Stoeber's method. Image analysis revealed that the particles are polydisperse in size (ranging from 300 nm to 2 μm). Prior to the aggregation experiments, the samples passed through a sucrose density gradient column in order to obtain more monodisperse spheres. Hence, the average hydrodynamic particle size was determined by means of dynamic light scattering, using an ALV-5000/E correlator. The measurements showed a final size distribution with an average diameter of 0.58 μm and a polydispersity index of 0.12. On the other hand, the particle mass density was measured by equilibrium centrifugation in sucrose to be approximately $\rho_p \approx 3.6$ g/cm^3. In our previous paper we performed light scattering experiments using small magnetic polystyrene particles of 170 nm in size. In this case, sedimentation was found to be negligible during the experiments due to the relatively small size and low mass density of only 1.2 g/cm^3 of those particles. The time evolution of the average chain diffusion coefficient at different electrolyte concentrations was successfully described by the aggregation kernel given by Eq. (3) [10]. For the present work, however, we employ particles of increased size and mass density in order to observe sedimentation of the linear aggregates that will form. Hence, the chosen experimental system allows us to study coupled field-induced aggregation and sedimentation processes. Particles of an even higher mass density could have been employed. In this case, however, the Brownian movement would be negligible with respect to the expected sedimentation velocities.

The particles are a nanocomposite material: the inner components, roughly 10 nm in size maghemite particles, are extremely confined inside the silica spheres (almost close packed). The magnetic character of the particles arises from an iron oxide content of 65% in weight. Under a given diameter the magnetization vector of the inner particles fluctuates around the easy axis of magnetization, with a characteristic relaxation time (Néel relaxation time) [17]. Magnetization measurements confirm that the particles possess no remanent magnetization. Exposed to magnetic fields stronger than 200 kA/m, the particles reach a saturation magnetization M_s of approximately 125 kA/m. At the field strength of 3.9 kA/m employed in our work, however, we are in the linear regime of the magnetization curve, where the magnetization M is proportional to the applied magnetic field H, i.e., $M=\chi H$. From the magnetization curve, the magnetic susceptibility of our particles was estimated to be $\chi \approx 2.6$.

The aggregation processes were monitored directly with an inverted microscope (Leica DM IL) equipped with a Scion CCD (charge-couple device) video camera and a set of

lenses for magnification of 10, 20, 40, and 100. The particle suspensions were contained in sealed rectangular capillars with a cross section of 1.0 mm $\times$ 0.1 mm. The field of view of the microscope was 768×512 pixels, corresponding to an area of 620 μm $\times$ 420 μm and an observed sample volume of 2.64×10^{-5} cm^3. During the experiments, typically about 700 particles could be observed in the field of view. A large number of initial monomeric particles are essential for maintaining reasonable statistics for larger aggregates at long aggregation times. Furthermore, the relatively large depth of field available at low magnification (10$\times$) helped to keep the particles in focus despite of their random Brownian motion.

Charged surface silanol groups prevent particle aggregation through repulsive electrostatic interactions. A particle surface potential of 10 mV was obtained by means of electrophoretic mobility measurements. Several series of experiments have been performed at different concentrations of an indifferent 1:1 electrolyte KBr. The electrolyte was always added to the colloidal dispersion before exposing the samples to the magnetic field. In our previous paper, we observed that the growth behavior depended even on small variations of the electrolyte concentration [10]. Now, the electrolyte concentrations used for reducing the repulsive electrostatic interactions were 0.0 mM, 0.5 mM, and 1.0 mM. Under these electrolyte concentrations the systems remain stable when they are not exposed to the magnetic field. For higher electrolyte concentrations the particles start to aggregate to the glass interface. This is not surprising since reported surface charges for glass interfaces in aqueous solutions are usually smaller than the charge of colloidal particles [18]. In fact, the particle concentration was determined adding NaCl electrolyte at 20 mM to the samples. At this concentration, the electrolyte screens the electrostatic repulsion between the particles and the glass walls. In this way, all the particles appear stuck to the walls and monomer counting becomes quite straightforward.

Some exploratory experiments were performed at different particle concentrations. However, high concentrations made the images difficult to analyze during the first stages of the aggregation, and low concentrations made the statistics of the cluster-size distribution worse. Therefore, the employed concentration was finally chosen to optimize the image analysis process. For the measurements, the particles were diluted in water to a final concentration of 2.65×10^7 particles/cm^3, corresponding to a volume fraction of $\phi = 2.74 \times 10^{-6}$. In any case, according to the theoretical background (Smoluchowski's equation), the aggregation kernel does not depend on the particle concentration (as long as the particle concentration is within the range where the Smoluchowski equation is applicable, and the lateral chain-chain aggregation is avoided).

Aggregation was induced applying a uniaxial magnetic field oriented parallel to the ground. The field divergence was small enough so that significant particle migration was not observed during the experiments. In this configuration, the aggregates sediment with their longer axis orientated perpendicularly to the gravitational field. Typical examples of what could be seen in the microscope are shown in Fig. 1. As expected, the video camera images reveal tip-to-tip aggregation when the field is applied.

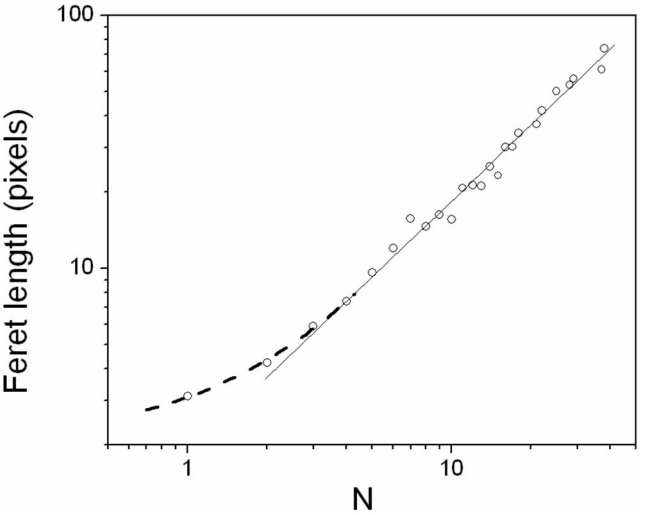

FIG. 2. Average Feret length of the clusters as a function of the chain size (data points). The continuous line shows linear fit for clusters larger than $N=3$. The quadratic fit for the shorter clusters is indicated by the broken line.

Due to the mass density mismatch, the particles used for our experiments settle due to gravity. If we had monitored the aggregation processes from above, the particles and linear aggregates might have reached the bottom of the sample chamber where they could have continued to aggregate but essentially in two dimensions. In order to study the pure three-dimensional case, we used the same experimental setup previously employed by Promislow *et al.* [7] who placed the microscope with its optical axes parallel to the ground. The longer axis of the sample tube is orientated parallel to the gravitational field vector. In this configuration, the aggregates can diffuse in all directions long before they can reach the bottom surface. Hence, aggregation takes place in the bulk where the diffusive particle motion is not restricted in any direction.

During the aggregation processes, digital images were taken in regular time intervals. As can be seen in Fig. 1, the individual particles and chainlike aggregates appear as dark spots and thin lines on a clear background. The length of individual clusters was analyzed using the public domain software "IMAGE-J" [19]. After subtracting the smooth continuous background, the images were thresholded in order to identify the particles and aggregates. The threshold level was automatically set by the IMAGE-J program based on an analysis of the gray level histogram of the image. Then, the program determined the Feret length of all the clusters detected on the image [20]. For the case of long linear clusters, Feret's length corresponds to the length of the aggregate axes. The program ignored aggregates touching the edge of the image since their total length is unknowable. Evidently, this effect introduced some extra but unavoidable noise on the cluster length histogram.

In order to correlate the Feret's length with the number of chain-forming particles, we compared different images obtained just before and after turning off the magnetic field. When the field is present, the clusters remain aligned along the field direction and the Feret length of the clusters can be

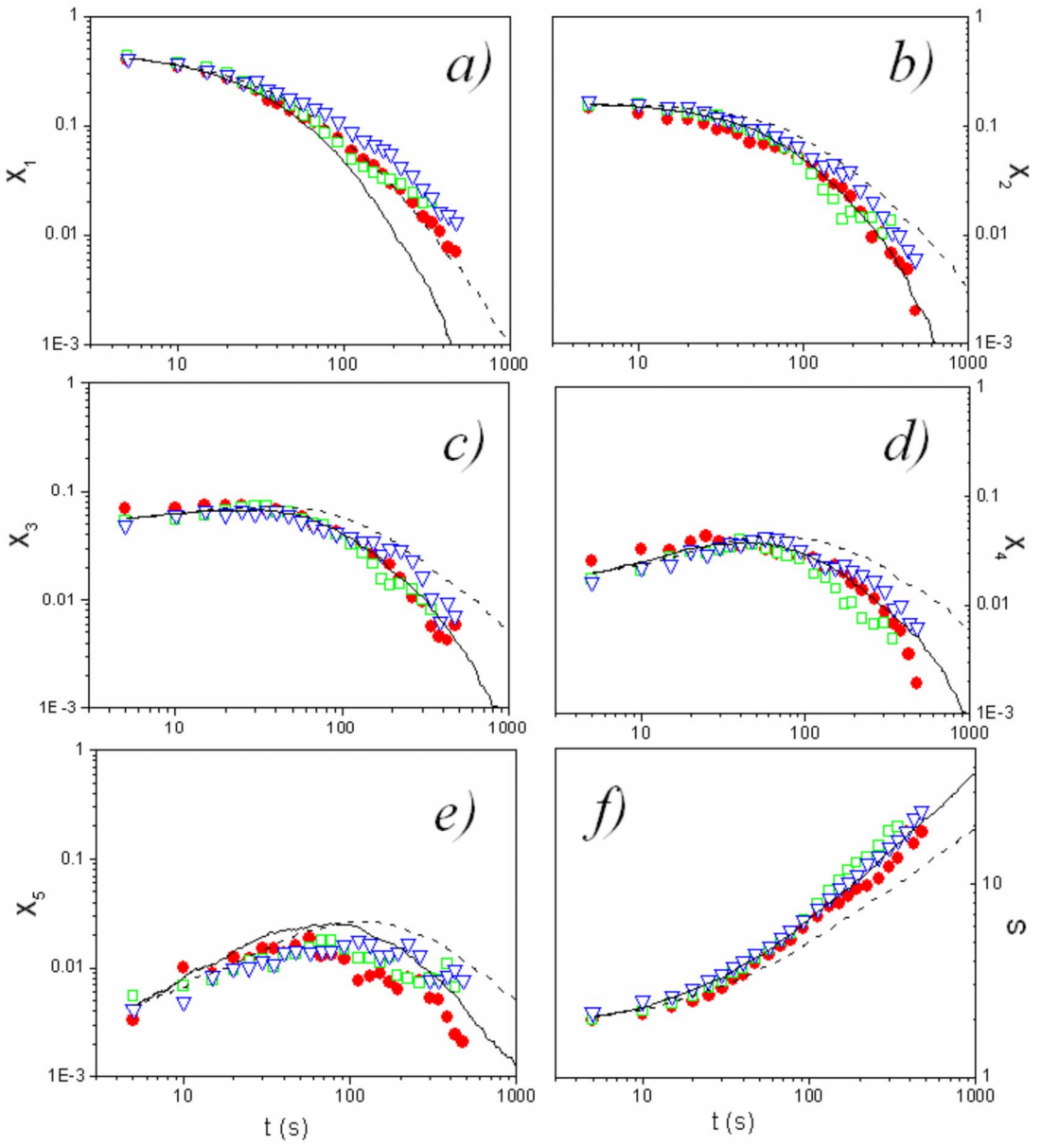

FIG. 3. (Color online) The figure shows the time evolution of the normalized cluster-size distribution at ●, 0 mM; □, 0.5 mM; and ▽,1.0 mM. The curves correspond to (a) monomers, (b) dimers, (c) trimers, (d) tetramers, and (e) pentamers. The dotted lines show the best fits using the aggregation kernel given by Eq. (3). The continuous lines show the same fit when differential sedimentation is taken into account. (f) also shows the time evolution of the weight-average chain length S as a function of the exposure time to the magnetic field at ●, 0 mM; □, 0.5 mM; and ▽, 1.0 mM. The continuous straight line shows the asymptotic behavior at long aggregation times. The corresponding kinetic exponent is $z=0.72$.

determined. When the field is turned off the clusters disassemble completely, and the number of chain-forming particles can be counted [cf. Figs. 1(c) and 1(d))] [21]. Figure 2 plots the Feret's length measured in pixels as a function of the number of particles per chain. For not-too-short chain lengths, a clear linear relationship was found. The best linear fit was obtained for $L_{\mathrm{Fer}}=1.84N+0.02$, where L_{Fer} is the Feret's length expressed in a number of pixels and N is the number of particles in the corresponding chain. For aggregates smaller than $N=4$, the linear relation is lost and the Feret's length is somewhat larger than what would be expected from the fit. This effect is probably due to the slightly blurred and consequently, not so clearly detectable border of the particles. In addition, digitalization effects may also play an important role. Evidently, these uncertainties are most pronounced for smaller chains when the cluster length comes close to the pixel size. We fitted to this part of the curve by a second order polynomial. The best fit was obtained for $L_{\mathrm{Fer}}=0.09N^2+0.98N+2.01$. Using both fitting equations, the cluster-size distribution and the average cluster size could be calculated for each image.

It should be noted that sometimes tiny spots appear on the image that may be caused by dust particles or noise. Since these spots are too small for being individual monomeric

particles, they had to be deleted from the cluster-size distribution. Therefore, we established a minimum Feret's length below which a detected particle was not taken into account. After a manual examination of the images, we established this level at 2.85 pixels or $N=0.8$ and kept it constant throughout the experiments. Nevertheless, particles and clusters that are about to drift out of the focal plane, e.g., may either not be detected or counted as smaller clusters. This effect introduces an extra error that makes an exact and univocal determination of the cluster size even more difficult.

Finally, the theoretical time evolution of the cluster-size distributions $X_i(t)$ was always obtained solving Smoluchowski's equation. Therefore, the stochastic algorithm described in Ref. [22] was employed. For this purpose, adequate kernel k_{ij} and initial conditions were considered.

IV. RESULTS

According to the experimental method described above, we monitored the aggregation processes that were induced in the sample due to the applied external magnetic field at different salt concentrations of KBr. Therefore, pictures were captured every 5 s during a total time interval of 495 s.

In Figs. 3(a)–3(e) we show the normalized cluster-size distribution for clusters formed by 1, 2, 3, 4, and 5 monomeric particles (pentamers) in logarithmic scale at different electrolyte concentrations (0.0 mM, 0.5 mM, and 1.0 mM). The data shown in the figure represent an average over four experiments. They are normalized by the initial number of particles. Errors bars are not included for the sake of clarity. In order to improve the data statistics and to reduce the number of data points to be plotted at longer aggregation times, several consecutive measurements were grouped and averaged accordingly. The number of clusters larger than pentamers became so low that statistical uncertainties and fluctuations prevailed and no meaningful curve could be drawn. For 0.5 mM and 1.0 mM electrolyte concentrations, the results superimpose and follow the curve observed at 0.0 mM. Contrary to the results reported in our previous work [10], where we observed that the growth behavior depends strongly on small variations of the electrolyte concentration; in this case the electrolyte does not affect the rate of the process.

Additionally, Fig. 3(f) shows the weight-average chain length $\langle S(t)\rangle=\Sigma_{n=1}^{\infty}n^2X_n/\Sigma_{n=1}^{\infty}nX_n$ as a function of the exposure time to the magnetic field at different electrolyte concentrations. The clusters of all sizes detected on the photos were taken into account for the average. Once more, the growth behavior does not depend on variations of the electrolyte concentration. In this logarithmic plot, $\langle S(t)\rangle$ shows a clear linear asymptotic behavior at long aggregation times and so, confirms the power-law behavior in the kinetics of aggregation. From the slope at long times, the experimental kinetic exponent z could be estimated to be $z=0.72$. This value agrees quite well with the results reported by Promislow *et al.* who obtained z values ranging from 0.51 to 0.75 for similar experimental conditions [7]. It is also close to the value of $z=0.67\pm0.04$ previously reported by our team for field-induced aggregation taking place at different electrolyte concentrations [10]. The kinetic exponent obtained for the theoretical curves is $z=0.58$, which is also very close to the value of $z=0.5$ deduced by Miyazima *et al.* for pure field-induced aggregation processes [6].

Before comparing fits with the experimental data, we would like to discuss the reason for not having imposed monomeric initial conditions at $t=0$ s. When no magnetic field is present, our superparamagnetic particles diffuse almost without any interaction. Only at relatively short interparticle distances, electrostatic repulsive forces avoid aggregation. Hence, a small fraction of monomeric particles may be so close to each other that they will be located within the attractive zone of the magnetic dipole interaction that appears as soon as the magnetic field is turned on. Due to the strong attractive magnetic forces, these particles will aggregate almost immediately when the field is turned on. An example of the result of such ballistic initial aggregation is shown in Fig. 1(a). Since such a transient effect is not described by Smoluchowski's equation, we were forced to impose as boundary conditions for the fits a cluster-size distribution that was measured after a sufficiently long time when the aggregation process becomes purely diffusion controlled [9]. Moreover, some small aggregates might initially be present before the magnetic field is applied. In order to fit the experimental results theoretically, we solved Smoluchowski's equation numerically using the aggregation kernel given by Eq. (3), and we imposed as boundary conditions the cluster-size distribution obtained at $t=5$ s. On the other hand, an affine transformation between the time in the simulation t_{sim} into the experimental one, t_{exp}, has been done $t_{\mathrm{sim}}=60\,t_{\mathrm{exp}}$. The transformation does not affect the curve shape at all in a log-log plot. It only introduces a horizontal shift of the data set as a whole. Hence, we can conclude that experimental and simulated times are functionally identical.

The theoretical results are plotted together with the experimental data in Figs. 3. The best fits for the experimental data shown in these figures were obtained for an average interaction range of $\bar{h}=4.35$ μm. This value is about 7.5 times the monomer diameter and is in good agreement with the long-range character of the dipolar magnetic interaction. It is, however, much larger than the values ranging from 1.89 to −0.21 times the monomer diameter that were reported in a previous study [10]. The relatively large range of the interactions observed now could explain why the growth processes do not depend significantly on the electrolyte concentration. The range of the total interaction between the particles may be controlled by varying the electrolyte concentration only when the outreach of the repulsive electrostatic interaction is sufficiently large and overcomes the range of the magnetic interactions substantially. Otherwise, the electrostatic part of the total interaction is negligible at large distances, and an effect of the electrolyte concentration on the aggregation kinetics is not expected. The measured magnetic moments and surface potentials of the particles agree clearly with the latter scenario. At the employed magnetic-field strengths, the magnetic moment of the silica particles is approximately 30 times larger than that achieved by the polystyrene particles in our previous work. On the other hand, their surface potential is approximately five times lower.

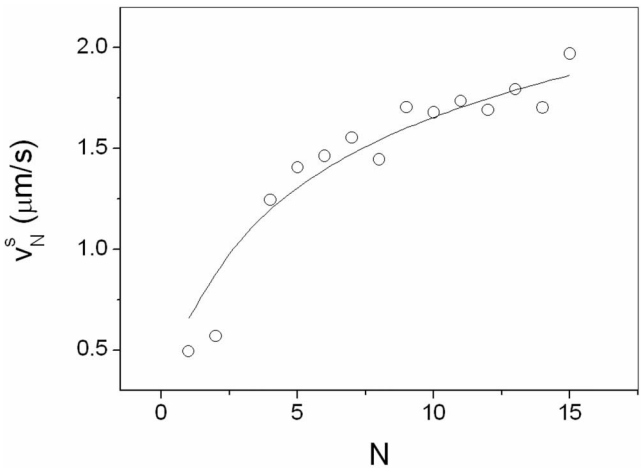

FIG. 4. Measured sedimentation velocities as a function of the chain length (data points). The continuous line shows the theoretical fit according to Eq. (5).

Although the trend is captured, the theoretical curves do not fit the experimental points. The theoretical predictions fit the experimental results well only during the first aggregation stages. After about 20 s, however, the fit and the experimental data start to differ noticeably. One possible reason for the mismatch between the theoretical predictions and the experimental results may be the influence of sedimentation. On the sequence of photos, it was clearly observable that the linear aggregates settle the faster the larger they grow. This means that the larger aggregates sweep a larger area than the smaller clusters and so, the collision frequency with other clusters is enhanced. During the first aggregation stages, this effect is negligible since there are only individual monomers and some smaller aggregates that settle at a relatively similar low average velocity. At longer aggregation stages, however, the differential sedimentation becomes more and more important. Since the aggregation kernel given by Eq. (3) does not account for this effect, it is not surprising that its predictions start to fail as the aggregates become larger.

In order to account for differential sedimentation, we determined the average settling velocities for monomers and aggregates using video microscopy and image processing. During the sedimentation velocity measurements, the magnetic field was present in order to maintain the linear structure and orientation of the chains. Figure 4 shows the measured average sedimentation velocities v_N^s as a function of the cluster size N. As can be seen, the monomer sedimentation velocity was $v_1^s \approx 0.5$ μm/s. This leads to a Péclet number of $\mathrm{Pe}=v_1^s a/D_0 \approx 0.17$. Since this number quantifies the relative strength of sedimentation and diffusion effects, we can conclude that thermal diffusion still dominates over sedimentation for the smaller particles. Nevertheless, Pe is not so small that sedimentation effects even for the monomeric particles may be neglected *a priori*.

We also measured the sedimentation velocities of the clusters and compared them with theoretical predictions. At low Reynolds number, the sedimentation velocity of a chain of length $2aN$, settling with its main axes oriented parallel to the ground, is given by $v_N^s=[N(4/3)\pi a^3 \Delta\rho g]/\zeta_\perp(N)$, where

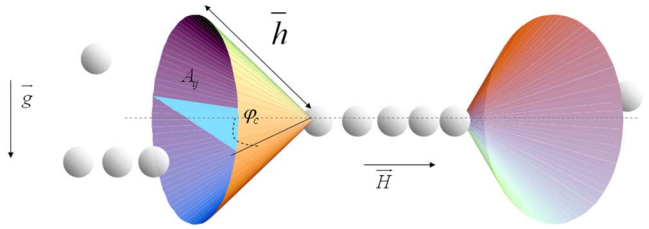

FIG. 5. (Color online) Schematic view of the attractive zone around a linear aggregate. Only clusters that are swept by the shaded circular sectors will aggregate due to sedimentation.

$\zeta_\perp(N)$ is the friction coefficient for movement perpendicular to the chain axis and $\Delta\rho=\rho_p-\rho_m$ is the density mismatch between the chain-forming particles and the continuous medium [23]. There are, however, no exact solutions for the friction coefficient of finite chains consisting of spherical particles. Nevertheless, chains of magnetic particles may be approximated by rigid cylinders of length L and diameter $2a$. In this case, the friction coefficient $\zeta_\perp(N)$ can be expressed as $\zeta_\perp(N)=(8\pi\eta aN)/[\ln(N)+\gamma_\perp(N)]$ and so, the sedimentation velocity becomes

$$v_N^s=\frac{\ln(N)+\gamma_\perp(N)}{6\eta}a^2\Delta\rho g. \tag{5}$$

The cylinder length function $\gamma_\perp(N)$ accounts for the so-called end-of-chain effects. According to Tirado and García de la Torre this chain end effect function is given by $\gamma_\perp(N)=0.84+0.18/N+0.24/N^2$ [16]. In spite of the fact that all the parameters in the analytic expression for the sedimentation velocity are fixed, we employed the average particle mass density ρ_p as a fitting parameter for the curve shown in Fig. 4. As can be seen, the theoretical curve fits the data satisfactorily and so, the theoretical expression given by Eq. (5) may be considered as a valid description for the sedimentation velocities of our chains. The best fit was obtained for $\rho_p=4.4$ g/cm^3. This value differs quite significantly from the value of $\rho_p=3.6$ g/cm^3 measured by equilibrium centrifugation in sucrose. Nevertheless, both values lie within the interval defined by the pure silica and iron oxide densities of $\rho=2.2$ g/cm^3 and $\rho=5.6$ g/cm^3, respectively. The observed discrepancy, however, could be caused by convective motion and back flow of the water. Previous studies have reported that the liquid-induced motion of the particles for a similar geometry could be of the order of $v \approx 1$ μm/s. Moreover, the fluid flow pattern suffers a distortion due to the presence of the container walls that will also affect the particles placed close to the walls. However, even when the cell width was large enough to avoid corrections due to wall effects, the sedimentation velocity of the linear aggregates could still be affected significantly due to convection and backflow effects [24].

For the additional contribution to the aggregation kernel due to differential sedimentation, the following kernel has been proposed in the literature [25]:

$$k_{ij}^s=A_{ij}|v_i^s-v_j^s|. \tag{6}$$

Here, A_{ij} is the combined cross section for aggregates of size i and j that settle with an average velocity of v_i^s and v_j^s,

respectively. For two spherical particles of radii R_i and R_j, the combined cross section A_{ij} is given by $A_{ij}=\pi(R_i+R_j)^2$. For linear magnetic clusters, however, the cross section does not depend on the cluster size since the chains essentially aggregate end to end. Considering the previously defined effective attractive zone of range $\bar{h}$ and aperture angle φ_c (see Fig. 5), the combined cross section becomes

$$A_{ij}=2\varphi_c(a+\bar{h}+a)^2. \tag{7}$$

This result allows the cluster-size distribution arising in coupled aggregation-sedimentation processes to be obtained theoretically using as aggregation kernel the expression $k_{ij}=k_{ij}^s+k_{ij}^{\mathrm{mag}}$ in Smoluchowski's equation. Using the previously described procedure, the time evolution of the cluster-size distribution is again calculated. The results are plotted in Figs. 3(a)–3(e). The weight-average chain length $\langle S(t)\rangle$ was also determined, and is included in Fig. 3(f). Also here, the experimental cluster-size distribution measured at $t=5$ s was imposed as a boundary condition for the calculations. The sedimentation velocities were determined according to Eq. (5), and the previously obtained value of the effective range $\bar{h}$ was kept. Figure 3 shows clearly that the theoretical fits improve quite substantially when sedimentation effects are considered. If one takes into account that no additional fitting parameter was introduced, the fit for the weight-average chain length $\langle S(t)\rangle$ is now very satisfactory.

According to Fig. 3, the main differences between the fits and the experimental data are observed for the monomer population. Such an underestimation of the number of monomers was already reported by Fraden *et al.* [8] for dilute suspensions of micron-diameter particles confined to two dimensions. These authors attributed this effect to the two-dimensional nature of their sample. In this case, larger aggregates partition the space and isolate smaller clusters on either side from each other. Hence, there will be more monomers left in the sample than predicted theoretically and a crossover from a two- to a one-dimensional behavior will take place. In our three-dimensional sample, however, a transition of this nature is not expected. The relatively large number monomers determined experimentally may, however, be due to detection problems since the size of these particles is just of the order of one image pixel. This implies that dust particles or aggregates that are not in the focal plane may erroneously be counted as monomers. Nevertheless, our data make clear that the agreement between the theoretical predictions calculated according to Smoluchowski's theory and the experimental results improve substantially when the sedimentation effects are considered. Especially, the asymptotic behavior of the weight-average chain length could be reproduced and the theoretically assessed kinetic exponent of $z=0.77$ comes quite close to the experimental value of $z=0.72$. This means that higher z values may be a sign of additional aggregation due to differential sedimentation.

The relatively large number of monomers that apparently are left behind in the aggregation process seem to indicate that the larger chains are more reactive than predicted by theory. One possible effect that could cause such behavior is mutual induction between the chain-forming particles. Zhang *et al.* have shown that mutual induction in the weak field regime may enhance the magnetization of a particle by up to 34% beyond the magnetization that it would have as an isolated single particle [13]. For a particle contained within an infinite chain of identical particles, the magnetic moment normalized by the magnetic moment of an isolated particle m_0 is

$$\frac{m}{m_0}=\frac{1}{1-\frac{4\zeta(3)}{3}\left(\frac{a}{d}\right)^3\chi}, \tag{8}$$

where $\zeta(3)=\Sigma_{n=1}^{\infty}1/n^3=1.22$ is the Riemann function, d is the distance between the particle centers, and χ is the magnetic susceptibility. Equation (8) must be adapted to finite chains before it may be applied in aggregation theory. The magnetic moment of the particles placed at the chain ends may be assessed imposing the following three approximations: (i) the chain-forming particles are in close contact, i.e., $d=2a$, (ii) all the chain-forming particles have an identical magnetic moment, and (iii) the infinite sum in the Riemann function $\zeta(3)$ may be truncated at $n=j-1$. Since the range of the magnetic dipole interaction scales as $\bar{h}\propto m^{2/3}$ [7], it is straightforward to deduce the following approximation for $\bar{h}$:

$$\frac{\bar{h}_{ij}}{\bar{h}_{11}}=\frac{1}{\left(1-\frac{\zeta_j(3)}{6}\chi\right)^{2/3}} \quad \text{for } j>i, \tag{9}$$

where $\zeta_j(3)=\Sigma_{n=1}^{j-1}1/n^3$. This means that the effective range of the net interaction depends on the aggregate size. In order to check the influence that mutual induction may have on the aggregation kinetics, we solved Smoluchowski's equation using this expression for the size dependency of the range of the magnetic dipole interaction. As before, the same boundary conditions and aggregation kernel ($k_{ij}=k_{ij}^s+k_{ij}^{\mathrm{mag}}$) were imposed. The best fits for the experimental data were now obtained for an average interaction range of $\bar{h}_{11}=2.61$ μm. Nevertheless, the fits remain almost unchanged and do not improve significantly with respect to the curves obtained before. This means that mutual induction within the chainlike aggregates increases the average range of the particle interaction. However, it seems to have no perceptible influence on the aggregation kinetics. Hence, mutual induction cannot explain why such a large number of monomers is left over.

V. CONCLUSIONS

We monitored field-induced aggregation processes arising in superparamagnetic particle suspensions using optical microscopy. The cluster-size distributions and the weight-average cluster were obtained from the recorded micrographs using image processing. We contrasted the time evolution of the cluster-size distribution with theoretical predictions given by Smoluchowski's equation. The latter equation has been solved using a recently proposed aggregation kernel which takes into account the anisotropic character and the long range of the net particle interaction. The experimentally assessed cluster distributions and the weight-average chain

length, however, match the theoretical predictions only during the first stages of aggregation. Including sedimentations effects, the fits improve substantially and the kinetic exponent of the fits ($z=0.77$) comes quite close to the experimentally obtained value of $z=0.72$. Hence, a relatively high value of z may be a sign of additional aggregation due to differential sedimentation. The time evolution of the monomer concentration, however, could not be reproduced satisfactorily. One reason for this finding may be the relatively large uncertainties that are introduced when processing images of small particles. Other reasons, however, cannot be excluded. We also checked the effect of the electrolyte concentration, but we did not find any influence on the aggregation kinetics. Finally, we determined an aggregation kernel that considers also the effect of mutual induction between the chain-forming particles. Mutual induction varies the average range of the particle interaction. However, it seems to have no perceptible influence on the aggregation kinetics.

ACKNOWLEDGMENTS

Financial support from the Spanish Ministerio de Educación y Ciencia [Plan Nacional de Investigación Científica, Desarrollo e Innovación Tecnológica $(I+D+i)$], projects No. MAT2006-12918-C05-01 and No. MAT2006-13646-C03-03, the European Regional Development Fund (ERDF), the Acción Integrada (Project No. HF2007-0007), and the Junta de Andalucía (Excellency Project No. P07-FQM-2496) is gratefully acknowledged. We also wish to thank Dr. Gerardo Odriozola for kindly providing the code of the stochastic method.

[1] A. M. Furst and A. P. Gast, Phys. Rev. E **62**, 6916 (2000).
[2] V. Cabuil, *Preparation and Properties of Magnetic Nanoparticles*, Encyclopedia of Surface and Colloid Science (Marcel Dekker, New York, 2004).
[3] R. Dreyfus, J. Baudry, M. L. Roper, M. Fermigier, H. A. Stone, and J. Bibette, Nature (London) **437**, 862 (2005).
[4] S. L. Biswal and A. P. Gast, Anal. Chem. **76**, 6448 (2004).
[5] L. Cohen-Tannoudji, E. Bertrand, L. Bressy, C. Goubault, J. Baudry, J. Klein, J. F. Joanny, and J. Bibette, Phys. Rev. Lett. **94**, 038301 (2005).
[6] S. Miyazima, P. Meakin, and F. Family, Phys. Rev. A **36**, 1421 (1987).
[7] J. H. E. Promislow and A. P. Gast, J. Chem. Phys. **102**, 5492 (1995).
[8] S. Fraden, A. J. Hurd, and R. B. Meyer, Phys. Rev. Lett. **63**, 2373 (1989).
[9] S. Melle, M. A. Rubio, and G. G. Fuller, Phys. Rev. Lett. **87**, 115501 (2001).
[10] F. Martínez-Pedrero, M. Tirado-Miranda, A. Schmitt, and J. Callejas-Fernández, Phys. Rev. E **76**, 011405 (2007).
[11] F. Martínez-Pedrero, M. Tirado-Miranda, A. Schmitt, and J. Callejas-Fernández, J. Chem. Phys. **125**, 084706 (2006).
[12] InSPACE is a microgravity fluid physics experiment that was operated on the International Space Station (ISS) in the Microgravity Science Glovebox from late March 2003 through early July 2003. (InSPACE is an acronym for investigating the structure of paramagnetic aggregates from colloidal emulsions.) The purpose of the experiment was to obtain fundamental data about the complex properties of magnetorheological (MR) fluids. The microgravity environment on the space station avoided the sedimentation effects, which otherwise would have become significant for the relatively large aggregates formed. Further details about this experiment are available at http://www.grc.nasa.gov/WWW/RT/2003/6000/6712agui.html
[13] H. Zhang and M. Widom, Phys. Rev. E **51**, 2099 (1995).
[14] H. Sonntag and K. Strenge, *Coagulation Kinetics and Structure Formation* (Plenum Press, New York, 1987).
[15] M. von Smoluchowski, Z. Phys. Chem., Stoechiom. Verwandtschaftsl. **92**, 129 (1917).
[16] M. Tirado and J. García de la Torre, J. Chem. Phys. **71**, 2581 (1979).
[17] L. Néel, Ann. Geophys. **5**, 99 (1949).
[18] S. H. Behrens and D. G. Grier, J. Chem. Phys. **115**, 6716 (2001).
[19] The public domain software "IMAGE-J" is available on the Internet at http://rsb.info.nih.gov/ij/index.html
[20] The Feret length is defined by the software manual as the largest distance measured between two parallel lines that are tangent to the boundary of an object detected on the image. It is also known as caliper length.
[21] Once the field is removed, the magnetic interaction vanishes due to the superparamagnetic character of most magnetic colloids. Therefore, if the aggregation takes place in a secondary minimum of energy the particles redisperse immediately, i.e., the rupture of the chains is observed (please see Refs. [5] and [11]).
[22] G. Odriozola, A. Schmitt, J. Callejas-Fernández, R. Martínez-García, and R. Hidalgo-Alvarez, J. Chem. Phys. **111**, 7657 (1999).
[23] G. K. Batchelor, J. Fluid Mech. **44**, 419 (1970).
[24] K. Zahn, R. Lenke, and G. Maret, J. Phys. II **4**, 555 (1994).
[25] G. Odriozola, R. Leone, A. Moncho-Jorda, A. Schmitt, and R. Hidalgo-Alvarez, Physica A **335**, 35 (2004).